

Troxel, S. W., Delanoy, R. L., "Machine Intelligent Approach to Automated Gust Front Detection for Doppler Weather Radars", Proc. SPIE, Vol. 2220, Jacques G. Verly, Sharon S. Welch, Editors, pp. 182-193, 1994.

Copyright 1994 Society of Photo-Optical Instrumentation Engineers. One print or electronic copy may be made for personal use only. Systematic reproduction and distribution, duplication of any material in this paper for a fee or for commercial purposes, or modification of the content of the paper are prohibited.

DOI: <http://dx.doi.org/10.1117/12.179602>

# Machine intelligent approach to automated gust front detection for Doppler weather radars\*

Seth W. Troxel and Richard L. Delaney

Massachusetts Institute of Technology / Lincoln Laboratory  
244 Wood Street, Lexington, MA 02173-9108

## ABSTRACT

Automated gust front detection is an important component of the Airport Surveillance Radar with Wind Shear Processor (ASR-9 WSP) and Terminal Doppler Weather Radar (TDWR) systems being developed for airport terminal areas. Gust fronts produce signatures in Doppler radar imagery which are often weak, ambiguous, or conditional, making detection and continuous tracking of gust fronts challenging. Previous algorithms designed for these systems have provided only modest performance when compared against human observations. A Machine Intelligent Gust Front Algorithm (MIGFA) has been developed that makes use of two new techniques of knowledge-based signal processing originally developed in the context of automatic target recognition. The first of these, functional template correlation (FTC), is a generalized matched filter incorporating aspects of fuzzy set theory. The second technique is the use of "interest" as a medium for pixel-level data fusion.

MIGFA was first developed for the ASR-9 WSP system. Its design and performance have been documented in a number of earlier reports. This paper focuses on the more recently developed TDWR MIGFA, describing the signal-processing techniques used and general algorithm design. A quantitative performance analysis using data collected during recent real-time testing of the TDWR MIGFA in Orlando, Florida is also presented. Results show that MIGFA substantially outperforms the gust front detection algorithm used in current TDWR systems.

## 1. INTRODUCTION

A gust front is the leading edge of a cold air outflow from a thunderstorm. The outflow, which is deflected at the ground, may propagate many miles ahead of the generating thunderstorm, and may persist as an outflow boundary long after the original storm has dissipated. Gust fronts can have a significant impact on air terminal operations since they often produce pronounced changes in wind speed and direction, forcing a change in active runway configuration and rerouting of aircraft already in the terminal airspace. In addition, wind shear, turbulence, and cross-winds along the frontal boundary pose significant safety hazards to departing and landing aircraft. Reliable detection and forecasting of gust fronts would both improve air safety and reduce costly delays. The Federal Aviation Administration (FAA) has sponsored research and development of automated gust front detection algorithms to be included as critical components of a suite of hazardous weather detection capabilities for the Airport Surveillance Radar with Wind Shear Processor (ASR-9 WSP) and the Terminal Doppler Weather Radar (TDWR) systems.

Gust fronts produce signatures that are observable to varying degrees in weather reflectivity and Doppler velocity data generated by Doppler weather radars. The first of these is the reflectivity thin line echo. The thin line is thought to be produced by a concentration of scatterers (dust, insects, rain droplets) along the leading edge of the outflow. The thin line varies in width but seldom exceeds 3 km. Typical reflectivities are in the range 5-20 dBZ<sup>†</sup>, but significant portions of many thin lines can have reflectivities as low as -10 dB. Because reflectivities along the thin line are so low, the thin line may appear broken in regions where return signal is below system noise, thereby making recognition and detection more difficult. The second signature is the velocity convergence signature. The air behind a gust front collides with air ahead of the front that may have markedly different velocities. In

---

<sup>†</sup> The basic unit of measurement for radar reflectivity is dBZ. Reflectivities of 50 dBZ or more are typical of intense thunderstorms with heavy rain. Clear air background typically has reflectivity values between -15 and 0 dBZ.

---

\* The work described here was sponsored by the Federal Aviation Administration. The United States Government assumes no liability for its content or use thereof.

a Doppler velocity image, this phenomenon is observable as a sharp transition in Doppler values when viewed along a single radial. A final key gust front signature is motion. When sequential radar scans are compared, convergence and thin line signatures of a gust front will move conspicuously in a direction perpendicular to the orientation of the convergence boundary and reflectivity thin line, while other features in the background scene (storm cells, ground clutter) are relatively stationary.

Examples of these gust front signatures can be seen in Figure 1, which shows corresponding reflectivity (left) and Doppler velocity (right) images from a single, near-horizon, 360-degree azimuth scan of the TDWR taken during an episode of summertime thunderstorm activity in Orlando, Florida. The radar is located at the center of the image and range rings are drawn at 20 km intervals out to 60 km. Several gust fronts evident in the imagery are indicated with overlaid white boxes. Several thunderstorm cells can be seen north and west of the radar. The storms north of the radar have produced two gust fronts. The first is propagating toward the west and has produced a thin line echo extending from roughly 25 km, 285 degrees to 55 km, 355 degrees. The velocity convergence signature is absent in this front because return signals from the clear air region ahead of the gust front was too low for the radar to measure. The second (weaker) gust front centered at 26 km, 75 degrees is moving to the east and is most evident as a zone of velocity convergence in the Doppler velocity image; note the abrupt transition from receding velocities (positive values) behind the gust front to approaching velocities (negative values) in the ambient air ahead of the gust front. Note also that in contrast with the first front, there is a velocity convergence signature but no discernible reflectivity thin line signature.



Figure 1. PPI images of radar reflectivity (left panel) and Doppler velocity (right panel) showing multiple gust front signatures. Range rings are in 20 km increments. Reflectivity is in dBZ. Doppler velocity is in m/s (dark grays indicate winds directed away from the radar, light grays indicate winds toward the radar). White boxes outline locations of gust fronts.

By examining images generated by these radars, experienced human observers can reliably detect and track gust fronts. However, the development of automated gust front detection algorithms having sufficiently high detection rates with few false alarms has been elusive. Current generation algorithms<sup>1,2</sup> are based on an approach developed nearly 10 years ago<sup>3</sup>. The traditional approach attempts to detect one or two signatures relying on techniques characterized by 1-dimensional (radial) signal processing, sequential thresholding of data, and complicated *ad hoc* heuristics. The gap between human and computer performance is arises out of several inherent limitations of the detection algorithms. These limitations include the lack of means for handling and maintaining weak, ambiguous, and contradictory evidence, the use of multiple pre-set thresholds for object discrimination (use of such thresholds can inadvertently result in the discarding of important data), a failure to use all of the relevant information available in the input data, and the ineffective use of knowledge regarding the behavior or appearance of gust fronts under different circumstances.

Given clear, unambiguous signatures, some of the existing automated detection algorithms perform reasonably well. The challenge is in constructing algorithms that can handle the marginally detectable ambiguous cases. In such cases, various factors must be considered. For example, gust front reflectivity signatures can be obscured by large areas of precipitation echoes. Doppler-based signatures are sensitive to the geometry between the winds being measured and the radar beam, vanishing when winds blow perpendicular to the beam (no radial component). Furthermore, gust front signatures can be mimicked by other natural phenomena, such as flocks of birds, clouds of dust, elongated bands of low-intensity rain, and ground clutter.

Machine intelligence techniques, originally developed at Lincoln Laboratory in the context of automatic target recognition, provide more effective means for exploiting, organizing, and assimilating such additional information<sup>4</sup>. These approaches to object recognition have been used to construct a Machine Intelligent Gust Front Algorithm (MIGFA) that is radically different from previous gust front detection algorithms. Versions of MIGFA have been developed for both ASR-9 WSP and TDWR systems. Results thus far clearly indicate that MIGFA substantially outperforms earlier approaches and, in some cases, is competitive with human observers. A detailed description of the ASR-9 WSP MIGFA can be found in [Delanoy and Troxel]<sup>5</sup>. This paper describes the more recently developed TDWR version of MIGFA.

## 2. LOW-LEVEL MACHINE INTELLIGENCE

### 2.1. Functional Template Correlation

Functional template correlation (FTC)<sup>6</sup> is a generalized matched filter that incorporates aspects of fuzzy set theory. Consider, as a basis for understanding, the basic image processing tool *cross correlation*. Given some input image  $I$ , an output image  $O$  is generated by matching a kernel  $K$  against the local neighborhood centered on each pixel location  $I_{xy}$ . The match score assigned to each pixel  $O_{xy}$  is computed by multiplying each element value of  $K$  by the superimposed element value in  $I$  and summing across all products. If the shape to be matched can vary in orientation, then the pixel  $I_{xy}$  is probed by  $K$  at multiple orientations. The score assigned to  $O_{xy}$  is the maximum across all orientations.

FTC is fundamentally the same operation with one important exception: whereas the kernel used in cross correlation is an array of image values (essentially a subimage of the image to be probed), the kernel used in FTC is an array of *scoring functions*. The scoring functions return scores that indicate how well the image values match the expectations of the values at each element of the kernel. The set of all returned scores are averaged and "clipped" to the continuous range [0,1]. The output of FTC is a map of these values, each of which reflects the degree of belief that the shape or object implicitly encoded in a functional template is present at that image location.

As an example, consider the functional template implementation of a simple matched filter designed to detect gust fronts in reflectivity data (Figure 2). Gust front thin lines are characterized by moderate reflectivity values (0 to 20 dBZ) that are flanked on both sides by low reflectivity (approximately -15 to 0 dBZ). The left side of Figure 2 shows the template kernel consisting of integers that correspond to the two scoring functions shown on the right. Elements of the kernel that do not correspond to either of the scoring functions form guard regions in which image (i.e., reflectivity) values are ignored and have no effect on match scores. Scoring function 0, corresponding to the flanking regions of low reflectivity, returns a maximal score of 1.0 for image values in the interval of -20 to -5 dBZ, a gradually decreasing score for image values in the interval -5 to 10 dBZ, and a score of -2.0 for image values larger than 10 dBZ. Scoring function 1, corresponding to the center of the kernel where moderate reflectivity values

are expected, returns maximal scores in the interval 5 to 12.5 dBZ and gradually decreasing scores for both higher and lower image values. Note that although very low image values can generate scores of  $-1.0$ , a slower decline in score with a minimum score of  $0.0$  is returned for image values above the maximal scoring interval. This asymmetry is an attempt to mitigate the obscuring effects of storm echoes and other patches of high reflectivity.

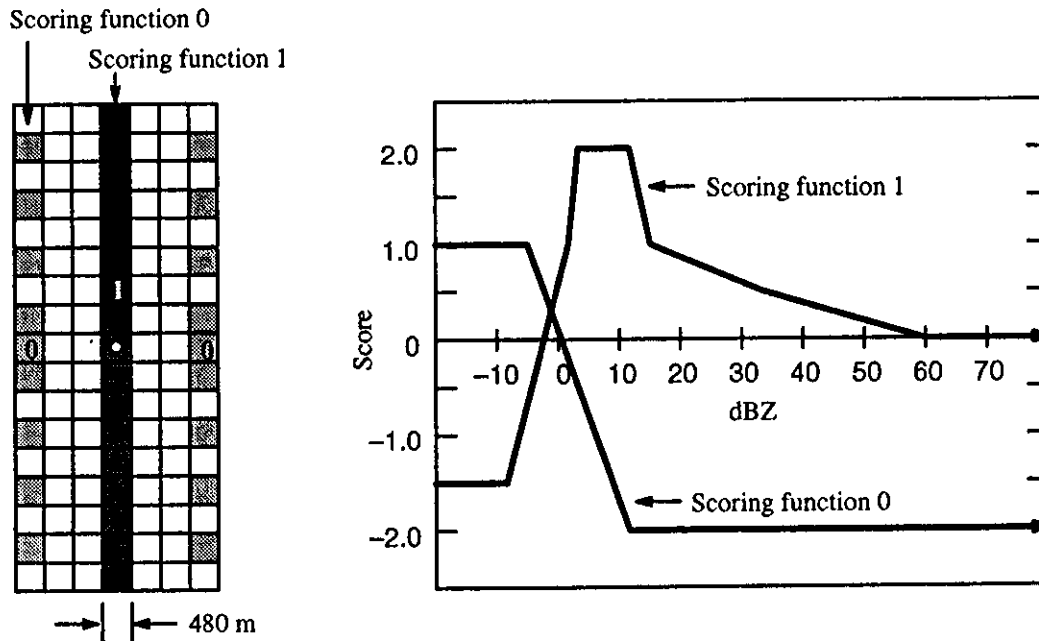


Figure 2. Example functional template for thin line feature detection. Input images are probed with the scoring array index kernel on the left. The indexes determine which scoring functions (right) are accessed (together with an underlying input image pixel) to return a match score at the input pixel location.

In general, by increasing or decreasing the intervals over which affirming scores (i.e., scores  $> 0.5$ ) are returned, scoring functions can encode varying degrees of uncertainty with regard to which image values are allowable. In addition, knowledge of how a feature or object appears in sensor imagery can be encoded in scoring functions. The interfering effects of occlusion, distortion, noise, and clutter can be minimized by the use of various design strategies.

## 2.2. Interest Images

Knowledge of the varying reliabilities of the selected feature detectors is used to guide data fusion and extraction. Conditional data fusion is simplified by using "interest" as a common denominator<sup>7</sup>. An interest image is a spatial map of evidence for the presence of some feature that is selectively indicative of an object being sought (the output of FTC is an interest as long as the functional template encodes an indicative feature). Higher pixel values reflect greater confidence that the intended feature is present at that location. Using interest as a common denominator, MIGFA fuses data by combining interest images derived from various pixel-registered sensory sources. Using simple or arbitrarily complex rules of arithmetic, fuzzy logic, or statistics, MIGFA can assimilate pixel-level evidence from several coregistered sources into a single combined interest image. Clusters of high values in such combined interest images are then used to guide selective attention and can serve as the input for object extraction. If done effectively, the combined interest image provides a better representation of object shape than is evident in any single sensor modality. Using these techniques, MIGFA performs a significant amount of knowledge-based processing before the application of the first discriminating threshold. Most traditional perception systems apply one or several thresholds early in the processing as a way of quickly reducing the amount of data to be processed. However, especially with ambiguous data, each applied threshold closes off options for detecting an object. A better strategy — a strategy used in MIGFA — is to apply thresholds only after evidence from many sources of information have been meaningfully fused into a single map of evidence.

### 3. MIGFA DESIGN

#### 3.1. Overview

The system block diagram in Figure 3 illustrates the configuration of the TDWR version of MIGFA. In preparation for processing, input images DZ (reflectivity) and V (Doppler velocity) from the current radar scan are converted from polar to Cartesian representation and scaled to a useful resolution. A map of shear (radial velocity change over a 1 km distance) is derived from input image V and serves as a third input image DV. The input images are then passed to multiple simple independent feature detectors that attempt to localize those features which are selectively indicative of gust fronts. The outputs of each of these feature detectors, most of which are based on some application of FTC, are expressed as interest images that specify evidence indicating where and with what confidence a gust front may be present. The different interest images are fused to form a combined interest image, thus providing an overall map of evidence indicating the locations of possible gust fronts.

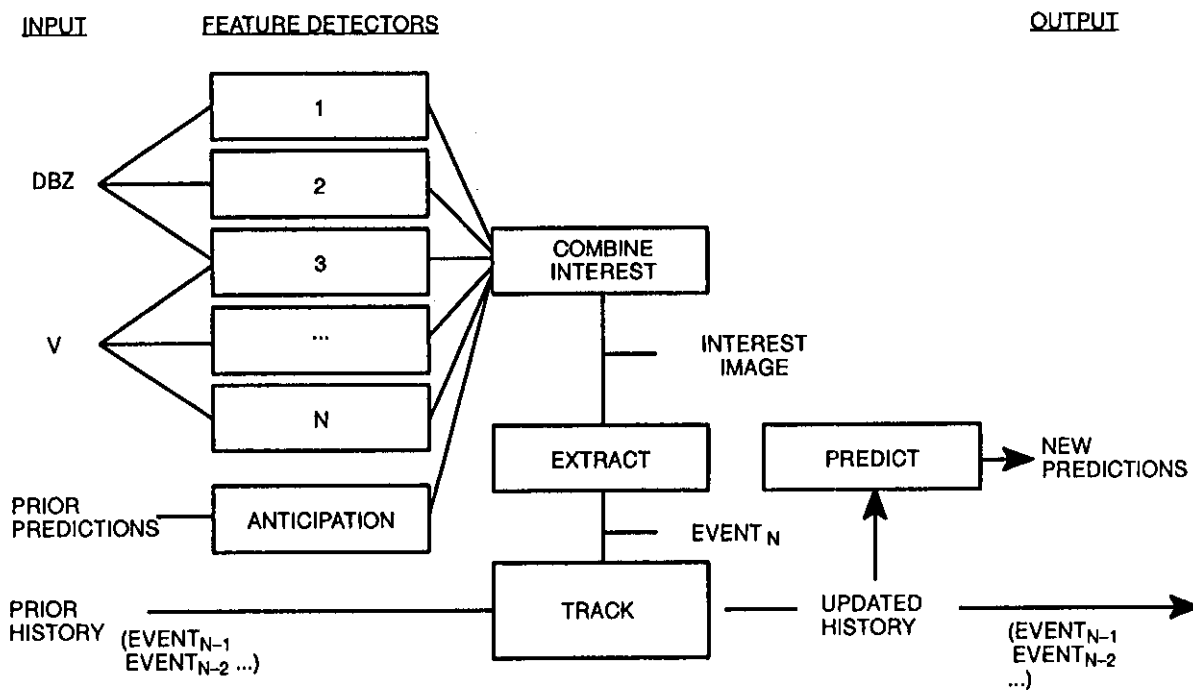


Figure 3. Block diagram of the Machine Intelligent Gust Front Algorithm (MIGFA).

From the combined interest image, fronts are extracted as chains of points. The chains extracted from a radar scan, collectively called an event, are integrated with prior events by establishing a point-to-point correspondence. Heuristics are then applied to reject those chain points which have an apparent motion that is improbable. The updated history is used to make predictions of where points along the front will be located as some future time. Such predictions are used in the processing of subsequent images, specifically in the feature detector called ANTICIPATION. In the output of ANTICIPATION, high interest values are placed wherever fronts are expected to be, thereby selectively sensitizing the system to detect gust fronts at specific locations. ANTICIPATION is tuned so that it will not automatically trigger a detection by itself but, when its output is averaged with other interest images, it will support weak evidence that would otherwise be insufficient to trigger a detection. Figure 4 is a summary of the processing steps for the input image shown in Figure 1.

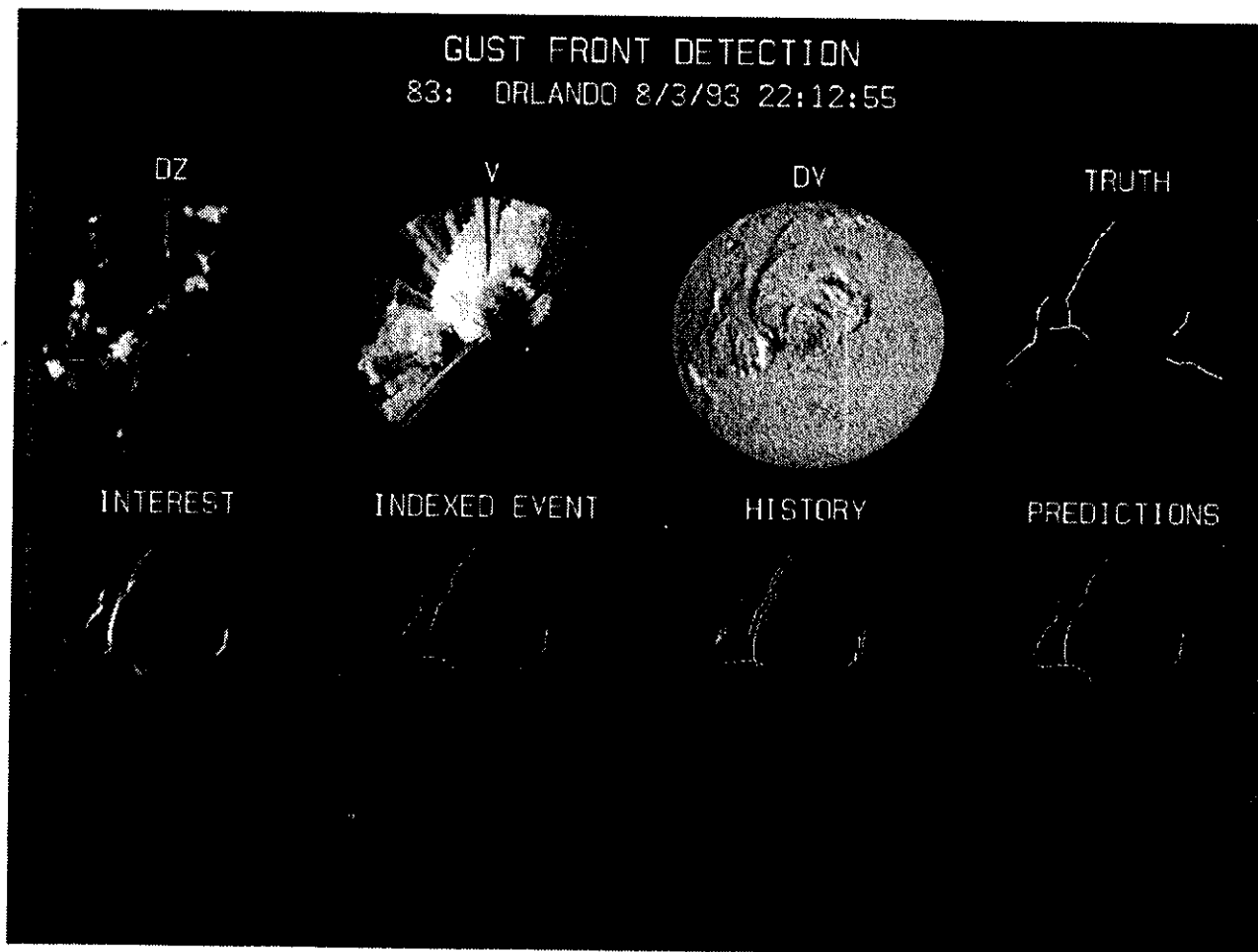


Figure 4. Processed scan summary. In the first row are the DZ (reflectivity) image, V (velocity) image, DV (velocity-change) image, and truth overlaid with bright white lines on the DZ image. The second row begins with the combined interest image computed from the DZ, V, and DV images. Next is the extracted indexed event. White pixels are those points which have been declared as part of a gust front. Gray pixels are those points which have not been tracked long enough to establish sufficient confidence. In the history frame, the current chain is shown in white and the preceding scans are shown in shades of gray (darker shades indicate more distant events in time). In the predictions frame, gray pixels indicate the 10- and 20-minute forecasts of where the fronts are expected to be, while white pixels indicate the current detected locations.

## 4. PROCESSING

### 4.1. Image preparation

As discussed earlier, a sharp change in velocity with distance (convergent velocity shear) is an indication of a gust front. To facilitate detection of convergent boundaries, missing values (arising from lack of signal or data quality editing by the radar system) in the input image V are first filled, where appropriate, by radially propagating neighboring pixel values. The cleaned velocity image is then used to derive a new image DV, where each pixel represents the local change in radial velocity over a 1 km range window centered on that pixel.

Pixel values for all images are scaled to the interval 0 to 255 to support subsequent FTC operations on the input imagery. Each image is tagged with the scaling factor and offset necessary to translate scaled values back to the original physical values. Finally, the input DZ, V, and derived DV images are converted from polar arrays (400 range bins  $\times$  360 radials) to Cartesian arrays (260

× 260). Mapping is done by computing for each element of the Cartesian array, the range bin and radial at which the corresponding value is to be found in the polar array. During the mapping process, an implicit subsampling of the data occurs. From an initial radial resolution of 149 m per range bin and pixel size in the azimuthal dimension decreasing from 1050 m at 60 km, the final Cartesian image has a pixel resolution of 480 m per pixel.

## 4.2. Feature detection

Given contextual information of the sensor being used, the location of that sensor, and the environmental conditions, a rule-based expert selects an appropriate set of feature detectors for application to the input data. For the moment, the only rule that is available chooses between two sets of feature detectors: one set customized for the ASR-9 WSP, the other for the TDWR. In fact, the two MIGFA versions are nearly identical, differing primarily in the set of feature detectors used. The TDWR MIGFA employs approximately ten different feature detectors, a few of which will be described here.

Figure 5 shows several interest images produced by applications of FTC to the input images displayed in the upper left. The figure also shows the combined interest image derived from all of the individual interest images. Homogenous, mid-level gray regions denote areas where specific feature detectors have not expressed an opinion regarding the presence of a gust front, deferring instead to the evidence generated by other feature detectors. The first interest image, labelled TDWR-TL-DZ-CONV, is generated by a tandem feature detector that looks for thin lines in the DZ image that are coincident and aligned with velocity convergence in the DV image<sup>†</sup>. Since obscuration prevents detection of thin line echoes inside storm cells, the TDWR-TL-DZ-CONV detector is prevented from generating opinions in these areas (unfounded negative opinions can inappropriately inhibit gust front detection). To mask storm regions from FTC operations, an image of storm regions is generated with a round functional template whose kernel has a diameter of 13 pixels (6.25 km) and whose associated scoring function returns high scores for high reflectivity pixels in the DZ image. Prior to applying FTC, the storm regions image is used to mask the input image by setting corresponding input image pixels to nil (i.e., no opinion).

The TDWR-DZ-CONV-MOTION detector is similar to TDWR-TL-DZ-CONV except that here we are looking for tandem motion of thin line and convergence features. Motion detectors are based on simple differencing. The DZ image from the previous scan (produced approximately 5 minutes before the current scan) is subtracted from the DZ image from the current scan. In the differenced DZ image, gust fronts appear as white lines (positive values at the front's position in the current scan) that are trailed by parallel dark lines (negative values at the front's position in the previous scan). Although functional templates that can scan for parallel white and dark thin lines simultaneously are feasible, these types of templates have so far proven to be too computationally expensive to operate within the real-time constraints of the available computer resources. The functional template used looks for thin lines of positive values and has a kernel that is identical to the one shown in Figure 2, but utilizes scoring functions that reflect the effects of image differencing. Treatment of the input DV image is similar except the order of differencing is reversed; the current scan is subtracted from the previous scan to produce positive values where moving convergence zones exist (convergence is indicated in single input DV imagery by negative values).

The interest image labelled TDWR-ASSORTED-MOTION represents the combined (logical OR) evidence from a number of single feature detectors. This constitutes a comparatively liberal detector that helps to offset the relatively conservative opinions produced by the tandem detectors. TDWR-CELL-CONVERGE and TDWR-CELL-CONV-MOTION look for static and moving velocity convergence boundaries respectively within storm regions. Note that all non-storm regions have been masked so that these detectors offer no opinions outside of storm regions.

The ANTICIPATION feature detector provides a mechanism for spatially adjusting the detection sensitivity of MIGFA on the basis of knowledge of various environmental data including the prior history of the gust fronts being tracked and dominant weather patterns. In particular, anticipation is used as a replacement for *coasting*, which is the continued tracking of an object for some time interval after the object's signal falls below threshold. Coasting works only when the target being tracked maintains a consistent velocity. But in reality, the reason the object signal falls below threshold is often because the object did change behavior. In contrast, anticipation works by creating bands of high interest values where the object is expected to be in the current scan.

---

<sup>†</sup> Briefly, a tandem detector generates a pixel score value by accumulating and averaging scores from simultaneous application of two (or more) functional templates to corresponding locations in the input images.

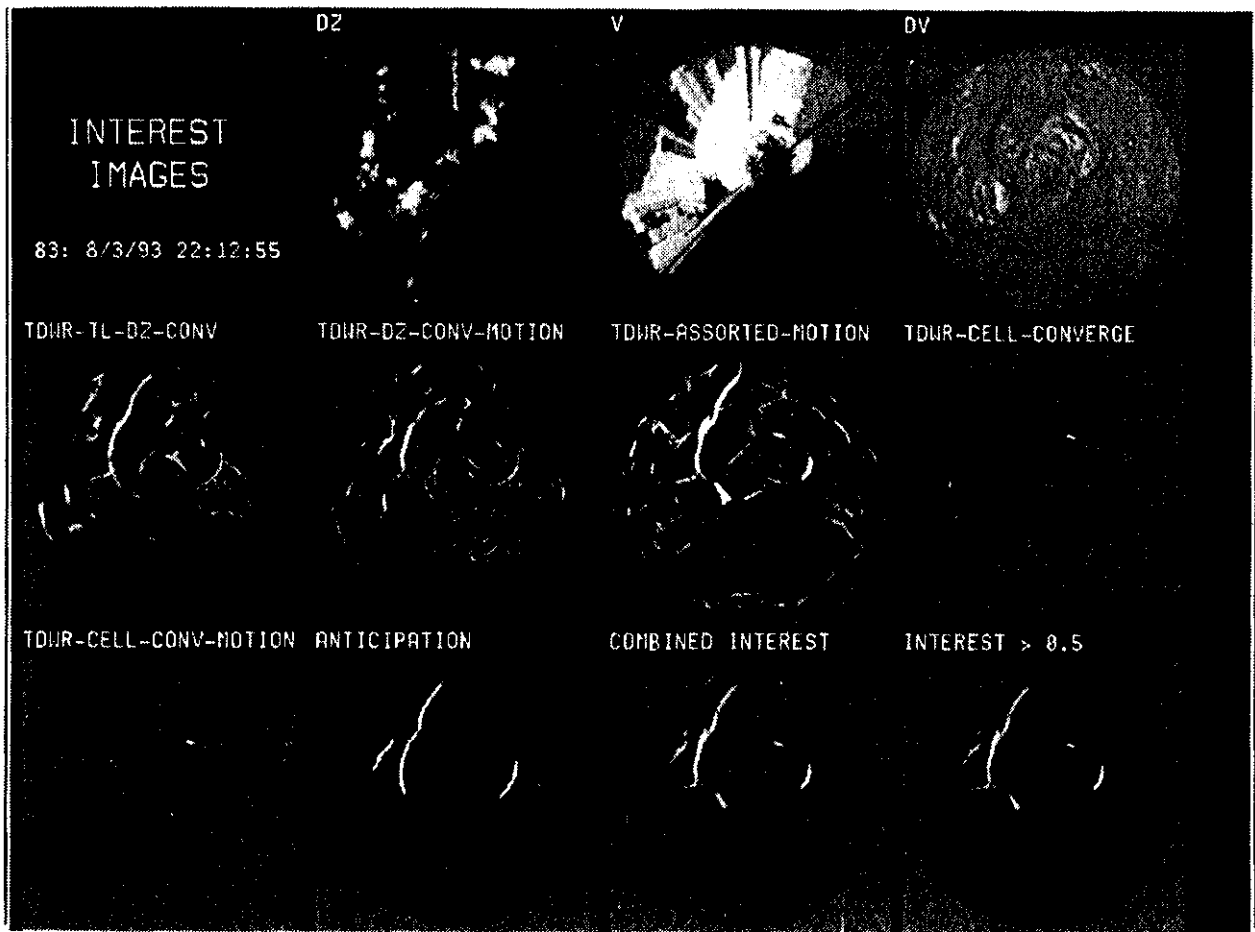


Figure 5. Combining of interest images. Input DZ (reflectivity), V (velocity), and DV (velocity change) images are shown along with output interest images from some of the feature detectors. The last two frames in the lower right show the images resulting from combining the various interest images.

Anticipation is set not so high as to trigger a detection by itself (i.e., coasting), but high enough to raise collocated weak signals above detection threshold.

#### 4.3. Combining evidence

In MIGFA, no one feature detector is meant to be a perfect, or even necessarily a good, discriminator of gust fronts and background. When used together, however, several weakly discriminating feature detectors can achieve robust performance depending on how the detector outputs are combined. The final combined interest image is generated by the assimilation of three major sources of evidence in a fairly complex rule of combination. The first major source is the evidence derived from clear air areas of the images. In this category are the two tandem feature detectors, TDWR-DZ-CONV-MOTION and TDWR-TL-DZ-CONV, which each provide a fairly conservative estimation of gust front locations. These are averaged with the more liberal TDWR-ASSORTED-MOTION image. Strong evidence that exists only in this last interest image would not be sufficient to trigger a gust front detection. However, when averaged with the two tandem feature detectors, the TDWR-ASSORTED-MOTION image does result in avenues of moderately high interest in the combined interest image through which extensions of gust front detections can be made.

The second major sources of evidence are from the feature detectors that generate interest within storm cells: TDWR-CELL-CONVERGE and TDWR-CELL-CONV-MOTION. The average of these two interest images are maximized with the clear air feature detectors to generate a map of image-derived interest.

The final combined interest image is the result of a weighted average of the image-derived interest with the ANTICIPATION interest image.

#### 4.4. Extraction

The goal of extraction in MIGFA is to identify the set of points (collectively called an *event*) that lie in *any* gust front. Individual points are tracked across time; the fact that a point belongs to one gust front or another is irrelevant to processing. MIGFA predictions are elastic in that the variable propagation velocities of different points along the gust fronts are each used to make predictions of what the gust front appearance and location will be at some time in the future.

Gust front features highlighted in the combined interest image may be fragmented due to combined effects of obscuration, data quality, and low return signal. To bridge gaps between collinear fragments and to suppress random unaligned high-interest values, MIGFA uses a special bow-tie shaped template to perform thin line smoothing of the combined interest image. The template, inspired by the receptive field of the cooperative cell of the Boundary Contour System developed by S. Grossberg and E. Mingolla<sup>8</sup>, weights the influence of the end regions over that of the center by placing more kernel elements at the ends. Consequently, the template generates high output interest scores for an image point between two collinear high-interest segments, even if that middle point itself has a low input interest value. A threshold of 0.5 is then applied to the smoothed image to create a binary image of candidate fronts. The elongated binary shapes that remain after thresholding are thinned down to a single-pixel-width skeleton by using an FTC implementation of a modified version of S. Levialdi's homotopic thinning<sup>9</sup>. In order to reasonably maximize detection length, the resulting chains are extended from their end points along ridges of relatively high interest values. After the chain-extension process has been completed, the resulting image may be highly branched and may contain loops. From each network of chain fragments is assembled the most interesting (typically, but not always, the longest) non-looping combination of chain segments.

#### 4.5. Tracking and Prediction

Tracking is done by establishing point-by-point correspondence between successive scans. For each point in the current scan, a point in the previous scan is found that is nearby and that has a propagation velocity consistent with the point in the current scan. Once correspondence is established, a link is created from the point in the current scan to its corresponding point in the previous scan. After indexing is completed, each extracted chain of points is edited in order to smooth the computed propagation speeds and orientations over local segments of the chains. Heuristics are then used to verify the detections, making use of knowledge of how gust fronts move. Chains exhibiting patterns of motion that are improbable are rejected.

The current extracted event, indexed into the prior history, is used to make predictions of where the points having sufficient depth and interest are likely to be at some time in the future. Given the direction moved, the propagation speed, and the current coordinates of an extracted point, a new coordinate is computed for some time in the future.

### 5. RESULTS

The TDWR MIGFA was installed on a Sun SPARCstation 10/30 equipped with 64 mbytes of RAM and was run in the Lincoln Laboratory TDWR testbed during real-time operations testing in Orlando, Florida in the summer of 1993. The algorithm ran 7 hours a day (minimum), 7 days a week, during most of the summer. During the same period, the current production TDWR algorithm (GF88) was also run, providing an opportunity for comparing the performance of the new algorithm against an existing standard. Performance of both algorithms was assessed by automated scoring of algorithm detections against a truth database generated by visual inspection of each input image processed by the two algorithms.

To generate the truth database, a human analyst had access to Doppler and reflectivity images for an entire sequence of TDWR scans, which could be viewed separately or in sequence as a movie. For each scan, the analyst entered a list of coordinates marking the gust front end points along with an intermediate sampling of points in between. For categorization of results, the estimated maximum wind shear in the convergence zone was also stored.

An automated scoring procedure, described in detail by Klinge–Wilson<sup>10</sup> compares computed gust front detections against coordinates contained in the truth database. Briefly described, the scoring algorithm connects the sequence of coordinates defining the limits of the gust front and expands the collection of spanning line segments into a 5–km wide region that is called a truth box. The scoring algorithm measures detection performance by two metrics. The first measure is a crude “hit/miss” statistic that counts a detection as successful if any part of the detection overlaps any part of a truth box. A detection is counted as false if it falls completely outside of any truth boxes. An overall probability of detection (POD) is computed by dividing the number of successfully detected fronts by the number of fronts identified by the human analyst. The probability of false alarm (PFA) is the number of false detections divided by the total number of detections (both valid and false). Probabilities are converted to percentages for reporting purposes. Detection quality was assessed by comparing the length of the front as estimated by each algorithm against the length identified by the human analyst. The percent length detected (PLD) is the length detected expressed as a percent of the length delimited by the human analyst. The percent of false length detected (PFD) reflects the fraction of total detection length that was not verified by truth.

Table 1 presents the automated scoring results and compares performance of MIGFA against GF88. Results were computed from a substantial database comprised of 230 hours of data collected on 30 different days during the test period. As can be seen from the table, MIGFA significantly outperformed the current TDWR gust front algorithm which uses more traditional signal processing techniques. MIGFA correctly detected and tracked over 70% of all gust fronts identified by human analysts, compared to approximately 30% for the existing algorithm. MIGFA does an even better job of detecting the overall length of gust fronts. MIGFA detected 66% of the total length of all gust fronts, representing a four–fold improvement over prior performance in this category. Note also that with both metrics, MIGFA significantly improves upon the false alarm rate. Of the nearly 2750 scans processed, false alarms occurred on only 54 scans with a resulting false alarm probability of only 3.5%

A significant fraction of the false alarms (and false detection length) issued by the gf88 algorithm were the result of coasting previous detections to maintain tracking during overhead passage (when velocity convergence signatures vanish). As discussed earlier, this is problematic since gust fronts do not always maintain their characteristics over the coasting period. They may speed up, slow down, or dissipate altogether. Since MIGFA does not use coasting, it does not suffer from this problem. The majority of MIGFA’s 7.5% PFD came directly from sporadic false detections (predominantly from leading edges of storm regions and thin, weak rain echoes) that were not associated with real gust front events. A small fraction (5–10%) of the PFD was due to inappropriate extension of some fronts beyond limits identified by the analyst. An equally small fraction of the PFD represents situations where the analyst was uncertain about the presence of a gust front, but decided not to generate truth for it; MIGFA may have been inappropriately penalized in some of these cases.

Table 1. Performance comparison between current (TDWR GF88) gust front detection algorithm and MIGFA .

	GUST FRONTS		GUST FRONT LENGTH	
	POD	PFA	PLD	PFD
TDWR GF88	29.5%	8.1%	12.8%	17.5%
MIGFA	71.2%	3.5%	65.7%	7.5%

Conceptually, it is easy to understand why MIGFA performs better. The current TDWR algorithm utilizes traditional 1–D processing of radial Doppler velocity convergence signatures as its primary means of detection. Without spatial context and additional information from other sources of evidence such as thin lines and motion, the GF88 algorithm is at a distinct disadvantage. Although some of the more recent algorithms do make use of thin line detection, modest improvements in detection probability have been accompanied by undesirably high false alarm probabilities. Once again, the traditional processing methods limit achievable performance gains.

## 6. CONCLUSIONS

The identifying signatures for gust fronts — thin lines of increased reflectivity, boundaries of converging Doppler values, and motion — are conceptually easy to describe and exploit as the basis for detection algorithms. And yet, although several research groups have worked collectively for nearly 10 years to develop reliable automatic gust front algorithms, none of the algorithms has demonstrated performance comparable to the ideal of human performance.

The problem is that automatic gust front detection, like other applications in computer vision, is deceptively much more difficult than the task of simply finding one or more signatures. Human observers use a variety of perceptual skills that have been notoriously and surprisingly difficult to implement in computer-vision systems. For example, humans use specific knowledge of the object being sought and the context of observation as well as the object's spatial and temporal context. The large performance gap between the performance of previous algorithmic approaches and humans in detecting gust fronts is in part due to the lack of these perceptual skills. These deficiencies are addressed in MIGFA through the use of machine intelligence at the lowest levels of processing, employing interest images as a mechanism for fusing evidence at the pixel level, 2-D signal processing (spatial context), motion (temporal context), fuzzy set theory (embodied in the use of FTC and interest images), and delayed thresholding.

MIGFA continues to undergo further field testing and development in both the ASR-9 WSP and TDWR systems. In addition, MIGFA is being enhanced to incorporate wind data from additional sensors within the Integrated Terminal Weather System (ITWS) currently under development by Lincoln Laboratory for FAA. ITWS seeks to integrate terminal weather information provided by various weather sensors and create aviation weather products suitable for air traffic control safety and planning functions. MIGFA's data fusion techniques lend themselves nicely to the ITWS concept. Finally, techniques used in MIGFA are being adapted to solve other meteorological detection problems, including microburst detection, microburst prediction<sup>11</sup>, and convective storm initiation.

## 7. ACKNOWLEDGEMENTS

The authors would like to thank Mark Isaminger and Mike Matthews who were responsible for overseeing MIGFA operations and logging results during real-time testing at the TDWR testbed site in Orlando, Florida. Their feedback was extremely valuable. Thanks also to Chris Keohan, who spent many hours examining TDWR data and generating the gust front "truth" database against which all algorithm results have been scored.

## 8. REFERENCES

1. L. Hermes, A. Witt, S. Smith, D. Klingle-Wilson, D. Morris, G. Stumpf, and M. Eilts, "The gust front detection and wind shift algorithms for the Terminal Doppler Weather Radar system," *J. Atmos. Oceanic Tech.*, Vol. 10, No. 5, 693-709, October, 1993.
2. M. Eilts, S. Olson, G. Stumpf, L. Hermes, A. Abrevaya, J. Culbert, K. Thomas, K. Hondl, and D. Klingle-Wilson, "An improved gust front detection algorithm for the TDWR," *Proc. 4th Intl. Conf. on the Aviation Weather System*, Paris, June 1991, p. J37.
3. H. Uyeda and D. S. Zrnic', "Automated detection of gust fronts," *J. Atmos. Oceanic Tech.* 3, 36, 1986.
4. J. G. Verly, R. L. Delanoy, and D. E. Dudgeon, "Machine intelligence technology for automatic target recognition," *Lincoln Laboratory Journal*, Vol. 2, No. 2, 277-311, 1989.
5. R. L. Delanoy and S. W. Troxel, "Machine intelligent gust front detection," *Lincoln Laboratory Journal*, Vol. 6, No. 1, 187-211, 1993.
6. R. L. Delanoy, J. G. Verly, and D. E. Dudgeon, "Functional templates and their application to 3-D object recognition," *Proceedings of the 1992 International Conference of Acoustics, Speech, and Signal Processing*, San Francisco, CA, March 23-26, 1992.
7. R. L. Delanoy, J. G. Verly, and D. E. Dudgeon, "Pixel-level fusion using interest images," *Technical Report TR-979*, MIT Lincoln Laboratory, Lexington, MA, May 1993.
8. S. Grossberg and E. Mingolla, "Neural dynamics of perceptual grouping: textures, boundaries, and emergent segmentations," *Perception and Psychophysics* 38, no. 2, 141, 1985.
9. S. Levialdi, "Parallel Pattern Processing," *IEEE Trans. Syst. Man Cybern.* 1, 292, 1971.
10. D. L. Klingle-Wilson, M. F. Donovan, S. H. Olson, and F. W. Wilson, "A comparison of the performance of two gust front detection algorithms using a length-based scoring technique," *Project Report ATC-185*, MIT Lincoln Laboratory, Lexington, MA, May 1992.
11. M. M. Wolfson, R. L. Delanoy, M. C. Liepins, B. E. Forman, and R. G. Hallowell, "The ITWS microburst prediction algorithm," *Preprints 5th Conference on Aviation Weather Systems*, Vienna, VA, August, 1993.